



HAL
open science

Changes in intermediate circulation in the Bay of Bengal since the Last Glacial Maximum as inferred from benthic foraminifera assemblages and geochemical proxies

Ruifang Ma, Sophie Sepulcre, Franck Bassinot, Laetitia Licari, Zhifei Liu, Nadine Tisnerat-Laborde, Nejib Kallel, Zhaojie Yu, Christophe Colin

► To cite this version:

Ruifang Ma, Sophie Sepulcre, Franck Bassinot, Laetitia Licari, Zhifei Liu, et al.. Changes in intermediate circulation in the Bay of Bengal since the Last Glacial Maximum as inferred from benthic foraminifera assemblages and geochemical proxies. *Geochemistry, Geophysics, Geosystems*, 2019, 10.1029/2018GC008179 . hal-02092589

HAL Id: hal-02092589

<https://hal.science/hal-02092589>

Submitted on 20 Jul 2021

HAL is a multi-disciplinary open access archive for the deposit and dissemination of scientific research documents, whether they are published or not. The documents may come from teaching and research institutions in France or abroad, or from public or private research centers.

L'archive ouverte pluridisciplinaire **HAL**, est destinée au dépôt et à la diffusion de documents scientifiques de niveau recherche, publiés ou non, émanant des établissements d'enseignement et de recherche français ou étrangers, des laboratoires publics ou privés.

Geochemistry, Geophysics, Geosystems

RESEARCH ARTICLE

10.1029/2018GC008179

Key Points:

- We produced high-resolution records of benthic foraminiferal assemblages, ^{14}C ages, oxygen, and carbon stable isotopes since 40 kyr BP
- Hydrological changes of the intermediate water in Bay of Bengal since LGM, were influenced by SSW during the LGM and NADW during the Holocene
- During the last deglaciation, geochemical records indicate increased northward flow of AAIW and enhanced upwelling in the Southern Ocean

Supporting Information:

- Supporting Information S1
- Table S1
- Table S2
- Figure S1

Correspondence to:

R. Ma,
rui-fang.ma@u-psud.fr

Citation:

Ma, R., S epulcre, S., Licari, L., Bassinot, F., Liu, Z., Tisn erat-Laborde, N., et al (2019). Changes in intermediate circulation in the Bay of Bengal since the Last Glacial Maximum as inferred from benthic foraminifera assemblages and geochemical proxies. *Geochemistry, Geophysics, Geosystems*, 20, 1592–1608. <https://doi.org/10.1029/2018GC008179>

Received 4 JAN 2019





Accepted 1 MAR 2019

Accepted article online 5 MAR 2019

Published online 27 MAR 2019

 2019. American Geophysical Union.
All Rights Reserved.

Changes in Intermediate Circulation in the Bay of Bengal Since the Last Glacial Maximum as Inferred From Benthic Foraminifera Assemblages and Geochemical Proxies

Ruifang Ma¹ , Sophie S epulcre¹, Laetitia Licari² , Franck Bassinot³ , Zhifei Liu⁴, Nadine Tisn erat-Laborde³ , Nejb Kallel⁵, Zhaojie Yu⁶, and Christophe Colin¹ 

¹GEOPS, Universit  Paris-Sud, CNRS, Universit  Paris-Saclay, Orsay, France, ²CEREGE, Aix-Marseille Universit -Europole de l'Arbois-BP80, Aix-en-Provence, France, ³LSCE/IPSL, CEA CNRS UVSQ, UMR 8212, Gif Sur Yvette, France, ⁴State Key Laboratory of Marine Geology, Tongji University, Shanghai, China, ⁵Laboratoire Georesources, Mat riaux, Environnements et Changements Globaux, LR13ES23, Facult  des Sciences de Sfax, Universit  de Sfax, Sfax, Tunisia, ⁶Key Laboratory of Marine Geology and Environment Institute of Oceanology, Chinese Academy of Sciences, Qingdao, China

Abstract Benthic foraminiferal assemblages and geochemical tracers ($\delta^{18}\text{O}$, $\delta^{13}\text{C}$ and ^{14}C) have been analyzed on benthic and planktonic foraminifera from core MD77-176, located in the northern Bay of Bengal, in order to reconstruct the evolution of intermediate circulation in the northern Indian Ocean since the last glaciation. Results indicate that during the Last Glacial Maximum (LGM), Southern Sourced Water masses were dominant at the core site. A high relative abundance of intermediate and deep infaunal species during the LGM reflects low oxygen concentration and/or mesotrophic to eutrophic deep water conditions, associated with depleted benthic $\delta^{13}\text{C}$ values. During the Holocene, benthic foraminiferal assemblages indicate an oligotrophic to mesotrophic environment with well-ventilated bottom water conditions compared with LGM. Higher values for benthic foraminifera $\delta^{13}\text{C}$ and B-P ^{14}C age offsets suggest an increased contribution of North Atlantic Deep Water to the northern Bay of Bengal during the Late Holocene compared to the LGM. Millennial-scale events punctuated the last deglaciation, with a shift in the $\delta^{13}\text{C}$ and the ϵ_{Nd} values coincident with low B-P ^{14}C age offsets, providing strong evidence for an increased contribution of Antarctic Intermediate Water at the studied site. This was associated with enhanced upwelling in the Southern Ocean, reflecting a strong sea-atmospheric CO_2 exchange through Southern Ocean ventilation during the last deglaciation.

1. Introduction

The thermohaline ocean circulation plays a key role in regulating climate changes at different time scales through heat redistribution and carbon cycling (e.g., Bryan et al., 2010; Rahmstorf, 1995; Stocker & Wright, 1996; Talley et al., 2011; Tomczak & Godfrey, 2003). It has recently been shown that a deep and vigorous overturning circulation may have persisted in the North Atlantic throughout most of the glacial period, only disrupted by episodes of sluggish circulation associated with the catastrophic iceberg discharge of the coldest Heinrich stadials (HS), the Dansgaard-Oeschger stadials, and the Younger Dryas cold event of the last termination (B hm et al., 2015). These major perturbations in Atlantic circulation have been related to the reduced North Atlantic Deep Water (NADW) flow (e.g., B hm et al., 2015; Mcmanus et al., 2004) and the advection of southern sourced waters (SSWs) filling a large part of the deep Atlantic ocean (e.g., B hm et al., 2015; Lynch-Stieglitz et al., 2007; Roberts et al., 2010).

Past changes in intermediate circulation are less well-documented than those of deep water (e.g., Kallel et al., 1988; Mix & Fairbanks, 1985; Oppo & Fairbanks, 1987; Waelbroeck et al., 2006). Previous studies of the intermediate water circulation during the last glaciation have mainly focused on the Atlantic Ocean (e.g., Lynch-Stieglitz et al., 2007; Oppo & Fairbanks, 1987; Pahnke et al., 2008) and the Pacific Ocean (e.g., Bostock et al., 2010; Mix et al., 1991; Pahnke & Zahn, 2005). These studies suggest an increased northward penetration of Antarctic Intermediate Water (AAIW) into the Pacific and Atlantic Oceans during glacial periods, as well as at a millennial time scale during the Heinrich events and stadials (e.g., Cao et al., 2007; Dubois-Dauphin et al., 2016; Pahnke et al., 2008; Pahnke & Zahn, 2005). In contrast, several studies based

on ϵ_{Nd} and Cd/Ca records (e.g., Came et al., 2008; Gu et al., 2017; Howe et al., 2016; Xie et al., 2012) suggest that no changes occurred or even that there was decreased northward penetration of AAIW during HS1 and the Younger Dryas. For the Southern Ocean, previous studies based on opal flux records (Anderson et al., 2009) and ^{14}C data (Skinner et al., 2010) have suggested an increase in the production and advection of AAIW during the LGM and the deglaciation, relative to the modern ocean, associated with more pronounced Southern Ocean upwelling. Thus, evidence for changes in the AAIW circulation through the last glacial period remains scarce and controversial, whereas changes in intermediate water masses need to be accurately constrained as they play a major role in regulating heat and salt distribution in the ocean and also affect the global climate through their influence on ventilation changes and atmosphere-ocean CO_2 exchange (e.g., Anderson et al., 2009; Skinner et al., 2010).

The Northern Indian Ocean is characterized by only weak vertical contrasts in physical properties of the water column due to a progressive vertical mixing of deep-water masses with intermediate ones. It plays an important role in global ocean circulation in terms of affecting the carbon storage capacity of the ocean and climate (e.g., Ahmad et al., 2008, 2012; Bryan et al., 2010; Raza et al., 2014; Talley et al., 2011). Compared to the Atlantic Ocean, only limited hydrographical observations have been carried out in the Indian Ocean due to its less distinguishable water mass characteristics, and little is known about the circulation below a depth of 1,000 m. Even though it has received increasing attention over recent decades (e.g., Bryan et al., 2010; Jung et al., 2009; Yu et al., 2018), the evolution through time of North Indian Intermediate and Deep Water (NIIW and NIDW, respectively) and the penetration of SSW into the North Indian Ocean, associated with changes of the large-scale thermohaline ocean circulation observed in the North Atlantic, are still poorly constrained for the period since the last glaciation and remain controversial (Naqvi et al., 1994; Ahmad et al., 2008, 2012; Bryan et al., 2010; Raza et al., 2014; Yu et al., 2018).

The Arabian Sea and the Bay of Bengal (BoB) are landlocked to the north by Asia. This land-sea configuration implies that much of the intermediate and deep waters of the northern Indian Ocean originate from the south, with only small contributions of intermediate waters from the Red Sea and of Pacific water to the Indonesian sea (Talley et al., 2011). Consequently, studying intermediate waters in the northeastern Indian Ocean will allow us to better constrain past changes in the production of intermediate and deep water and in circulation from the Southern Ocean; in addition, it will help us to understand their potential role in global climate changes (Jung et al., 2009; Kallel et al., 1988; Yu et al., 2018).

In this study, we have investigated benthic foraminiferal assemblages together with $\delta^{13}\text{C}$, $\delta^{18}\text{O}$, and ^{14}C of benthic foraminifera from core MD77-176, located in the BoB, in order to reconstruct hydrological changes in the intermediate waters at high temporal resolution over the last 40 cal kyr. Our results, combined with previous foraminifera ϵ_{Nd} obtained on the same core (Yu et al., 2018) and on several deeper cores in the BoB, allow us to constrain the temporal evolution of the source, ventilation and structure of intermediate and deep-water masses of the northern Indian Ocean and the northward penetration of AAIW.

2. Modern Hydrological Settings

Today, surface water above 100 m in the BoB results from a mix of Arabian Sea Surface Water and Bay of Bengal Water (Figure 1; Talley et al., 2011; Tomczak & Godfrey, 2003). Thermocline and intermediate-depth water masses are Indonesian Intermediate Water (IIW) and Red Sea Intermediate Water (RSIW). IIW originates from the Pacific Central Water and enters the BoB via the Indonesian through flow. IIW flows clockwise at thermocline levels in the BoB (You, 1998). RSIW is created by the outflow of water from the Red Sea and Persian Gulf into the Arabian Sea, where it can sink to depths of 400–1,400 m due to its high salinity (Talley et al., 2011). RSIW enters the BoB around the southern tip of India and also circulates in a clockwise direction (You, 1998). In the South Indian Ocean, Antarctic Intermediate Water (AAIW) is found at 1,000- to 1,500-m depth, just above Indian NADW (Tomczak & Godfrey, 2003). Today, the northward extension of AAIW in the Indian Ocean rarely reaches beyond 10°S (Lynch-Stieglitz et al., 1994).

The Indian Deep Water (IDW) lies between 1,500 and 3,800 m. It forms when the Circumpolar Deep Water admixes with NADW (Tomczak & Godfrey, 2003; You & Tomczak, 1993). At depths below 3,800 m, the Antarctic Bottom Water (AABW) only reaches the southern part of the BoB as most of the BoB is shallower than 4,000 m (Tomczak & Godfrey, 2003). However, AABW can also mix with the IDW and thus contributes

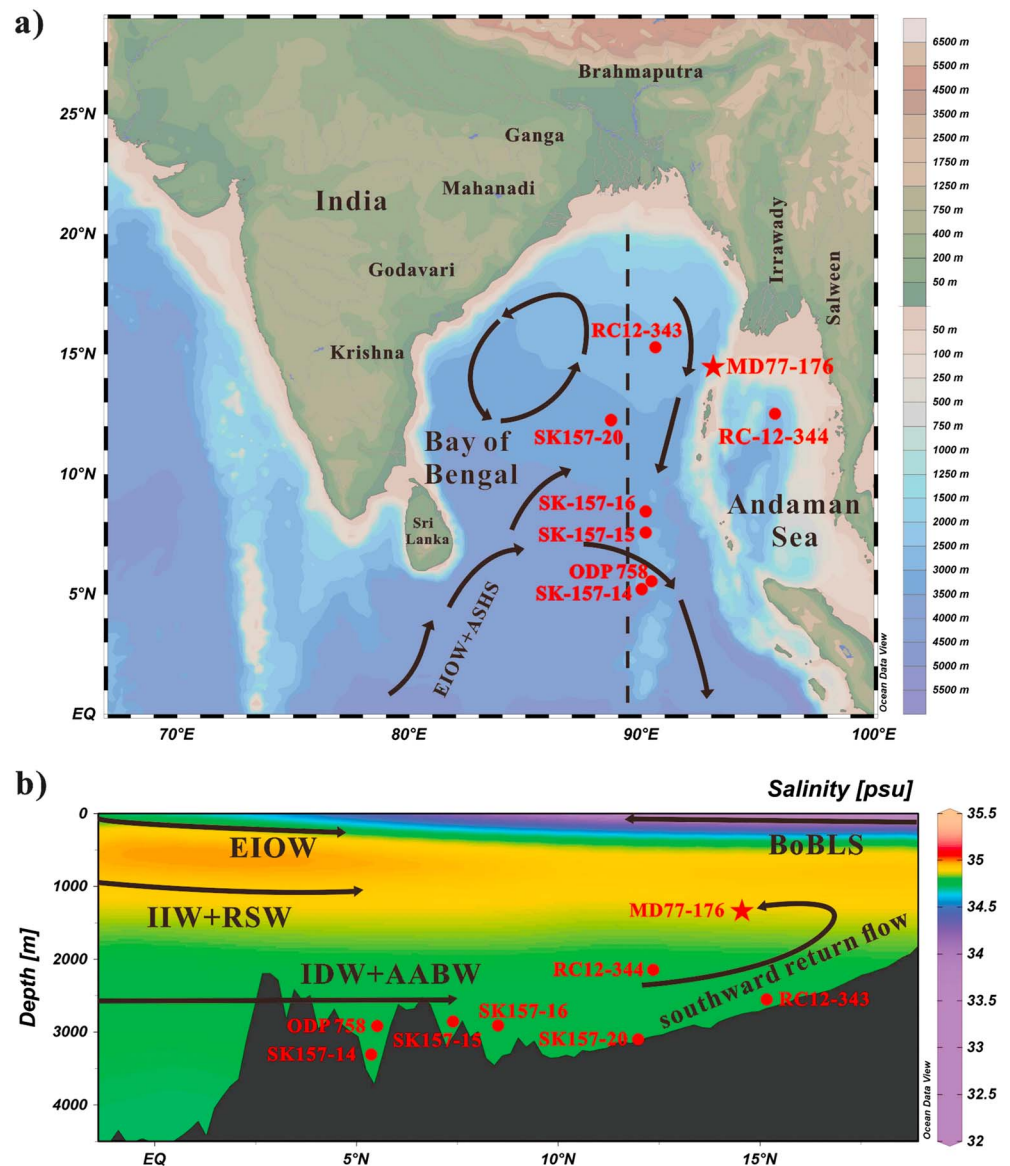


Figure 1. (a) Geographical setting and locations of reference sites (red circles) and MD77-176 (red star) in the Bay of Bengal. The black arrows show the general direction of surface circulation in the Bay of Bengal from June to September (Shankar et al., 2002). (b) Salinity (psu, colored shading) depth-latitude section using Ocean Data View (ODV) software (Schlitzer, 2015) and vertical distribution of water masses in the Bay of Bengal (N-S cross-section). EIOW = Eastern Indian Ocean Water; BoBLS = Bay of Bengal low salinity Water; IIW = Indonesian Intermediate Water; RSW = Red Sea Intermediate Water; AABW = Antarctic Bottom Water; IDW = Indian Deep Water.

significantly to the deep-water masses in the BoB. As the bottom water upwells when it moves northward, the deep waters can eventually return to shallower depths (Talley et al., 2011). Thus, changes in the bottom waters can also affect shallower-depth water masses in the northern BoB.

3. Material and Methods

3.1. Sediment Core and Age Model

Core MD77-176 was collected from 1,375-m water depth in the northeastern BoB (14°30'5N–93°07'6E; Figure 1). The sediment consists of intercalated olive gray terrigenous clay and silty clay layers with foraminifer- or nannofossil-bearing ooze. The age model of core MD77-176 was previously established by

using 31 planktonic foraminifer (*Globigerinoides ruber*) AMS ^{14}C dates combined with the MD77-176 oxygen isotope record obtained on planktonic foraminifera *G. ruber*, which were correlated to the GISP2 Greenland ice core record (Marzin et al., 2013). Core MD77-176 displays high accumulation rates (average ~ 25 cm/kyr and up to 40 cm/kyr for the Holocene) and could provide high-resolution records for the period since 40 cal kyr BP.

3.2. Methods

Samples were available from previous studies (Kallel et al., 1988; Marzin et al., 2013) and were sieved in the 63- to 150- and >150 - μm fractions. A total of 217 samples were collected for benthic foraminiferal analysis.

3.2.1. $\delta^{18}\text{O}$ and $\delta^{13}\text{C}$ Analyses

Measurements of $\delta^{18}\text{O}$ and $\delta^{13}\text{C}$ were performed on 191 samples of benthic foraminiferal species (supporting information Table S1). The $\delta^{18}\text{O}$ and $\delta^{13}\text{C}$ records covering the period since 14 cal kyr BP had previously been analyzed on benthic foraminifera *Cibicidoides wuellerstorfi* at the Laboratoire des Sciences du Climat et de l'Environnement (LSCE, France). These analyses were carried out on a Finnigan MAT 251 mass spectrometer, and the mean external reproducibility of carbonate standards is $\pm 0.05\text{‰}$ for $\delta^{18}\text{O}$ and $\pm 0.03\text{‰}$ for $\delta^{13}\text{C}$. In order to obtain high-resolution $\delta^{18}\text{O}$ and $\delta^{13}\text{C}$ records spanning the last 40 cal kyr BP, benthic foraminifera *Cibicidoides wuellerstorfi*, *C. pachyderma*, and *Uvigerina peregrina* were also analyzed at the State Key Laboratory of Marine Geology of Tongji University (Shanghai, People's Republic of China). Approximately four to eight clean and well-preserved specimens (>250 μm) were selected per sample. Stable isotope analyses were performed using a Finnigan MAT 253 mass spectrometer, with a mean external reproducibility better than $\pm 0.07\text{‰}$ for $\delta^{18}\text{O}$ and $\pm 0.04\text{‰}$ for $\delta^{13}\text{C}$. $\delta^{18}\text{O}$ and $\delta^{13}\text{C}$ values were calibrated versus Pee Dee Belemnite (PDB) by using National Bureau of Standards. The average time resolution of $\delta^{18}\text{O}$ and $\delta^{13}\text{C}$ obtained on benthic foraminifera is about 160 years for the Holocene and 1,100 years for the deglacial and the last glacial period.

3.2.2. Radiocarbon Dating of Benthic Foraminifera

Radiocarbon analyses were performed on epifaunal species *Cibicidoides* spp. and *Hoeglundina elegans* (size >150 μm). Approximately 400 to 1,000 μg of benthic foraminiferal shells were picked. They were leached with HNO_3 (10^{-2} M), rinsed with Milli-QTM water, converted to CO_2 by reacting with anhydrous phosphoric acid (Tisnérat-Laborde et al., 2001) and collected in small glass tubes (Wacker et al., 2013). Fourteen samples were analyzed with the ECHOMICADAS at the LSCE, France. Measurements were taken using the gas handling system and cracker system (Wacker et al., 2013). Radiocarbon results are reported as conventional ^{14}C ages in yr BP and the benthic-planktonic ^{14}C age offsets.

3.2.3. Faunal Analysis

For each sample, benthic foraminifera (>150 μm) were extracted, counted, and identified to species level following the taxonomical descriptions of various authors (e.g., Holbourn et al., 2013; Jones, 1994; Loeblich & Tappan, 1988). As bulk samples of core MD77-176 were not weighed, we could not calculate absolute abundance of foraminifera or accumulation rates. All specimens were counted, and individual census counts were expressed as the percentage of total benthic foraminifera present in each sample.

To describe major faunal variations, we performed principal component analysis using PAST software (Version 3.0, Hammer et al., 2001). Species with a percentage presence of $>1\%$ in at least one sample were used for statistical analysis and diversity calculation.

4. Results

4.1. Stable Isotope Results

We combined stable isotope analyses performed on *C. pachyderma*, *C. wuellerstorfi*, and *U. peregrina* in order to produce the most complete record possible. Vital effects on $\delta^{18}\text{O}$ and $\delta^{13}\text{C}$ of selected species have been extensively documented in several previous studies. *U. peregrina* is known to record the calcite $\delta^{18}\text{O}$ at equilibrium (e.g., Shackleton, 1974), whereas *C. wuellerstorfi* exhibits a vital effect ranging from 0.64‰ to 0.82‰ (Ahmad et al., 2012; Duplessy et al., 1984; Mackensen et al., 1993; Naqvi et al., 1994; Raza et al., 2014). As *U. peregrina* is an endobenthic species, its $\delta^{13}\text{C}$ cannot be used to reconstruct changes in the bottom water $\delta^{13}\text{C}$, whereas *C. wuellerstorfi* is known to record the $\delta^{13}\text{C}$ of bottom water (Duplessy et al., 1984; Zahn

Table 1
Stable Isotope Data (Per Mil Versus PDB) From the Core MD77-176 of *Cibicoides pachyderma*, *Cibicoides wuellerstorfi*, and *Uvigerina peregrina* in the Same Levels to Assess the Vital Effect and Microhabitat Effect for $\delta^{18}\text{O}$ and $\delta^{13}\text{C}$, Respectively

Depth (cm)	$\delta^{13}\text{C}$ (‰ versus PDB)		$\delta^{18}\text{O}$ (‰ versus PDB)	
	<i>Cibicoides pachyderma</i>	<i>Cibicoides wuellerstorfi</i>	<i>Cibicoides wuellerstorfi</i>	<i>Uvigerina peregrina</i>
30–33	0.30	0.42	1.80	2.61
35–38	0.07	0.39	1.91	2.88
40–43			1.88	2.69
45–48	0.12	0.42	1.97	2.97
50–53			2.00	2.72
55–58	0.09	0.42	2.00	2.94
65–68	0.26	0.47	2.09	
70	0.24	0.25	2.00	
80–83	0.20	0.44	2.09	
85–88	0.17	0.36	1.96	2.87
90	0.12	0.22	1.84	
170	0.33	0.28	1.89	
180	0.35	0.43	2.01	
185	0.25	0.24	1.72	
200	0.19	0.37	1.93	2.69
220	0.21	0.46	1.92	
230			1.94	2.78
280			2.01	2.84
300			2.02	2.85
585			3.23	3.75
930	−0.37	−0.29	2.88	3.74
940	−0.27	−0.36	2.87	3.87
970	−0.11	0.01	3.07	
980	−0.16	−0.09	3.12	3.66

et al., 1986) without any microhabitat effect (except in some particular areas, such as the Southern Ocean, Mackensen et al., 1993).

Most of the benthic $\delta^{13}\text{C}$ records were obtained from *C. wuellerstorfi*. In order to correct the $\delta^{13}\text{C}$ results from *C. pachyderma* to *C. wuellerstorfi*, we produced 18 pairs of measurements for certain levels where the two species coexisted (Table 1). Results indicate a slight difference in the stable isotopic composition (0.13‰ for $\delta^{13}\text{C}$). In addition, the results of 15 pairs of *C. wuellerstorfi* and *U. peregrina* measurements (Table 1) indicate a mean offset of about 0.82‰ in the $\delta^{18}\text{O}$ values. We corrected *C. wuellerstorfi* $\delta^{18}\text{O}$ values for this vital effect of 0.82‰ to establish a composite record combining results obtained on both species.

For core MD77-176, downcore benthic $\delta^{18}\text{O}$ values range between 2.48‰ and 4.23‰ (Figure 2). The most enriched $\delta^{18}\text{O}$ value (4.23‰) occurred in the last glacial maximum and the most depleted (2.48‰) in the late Holocene (3.5 cal kyr BP). In addition, during the later part of the deglaciation, the $\delta^{18}\text{O}$ showed a marked decrease at 11.5 kyr (2.51‰) followed by higher values during the early Holocene (mean value of 3.15‰ between 10.5 and 8 cal kyr BP), and then a decrease from 9.9 cal kyr BP to the core top (mean value of 2.83‰).

The $\delta^{13}\text{C}$ values range from −0.46‰ to 0.49‰ (Figure 2). Compared with the lower values (−0.13‰) for the LGM, a rapid increase in the $\delta^{13}\text{C}$ begins at 17 cal kyr BP, highlighting the end of the LGM. From 17 to about 10 cal kyr BP, the $\delta^{13}\text{C}$ record exhibits a succession of large oscillations with a first wide peak (0.1‰) occurring between 17 and 14 cal kyr BP, and a second shorter maximum (0.15‰) between 13 and 10.5 cal kyr BP. During the Holocene, the mean value of $\delta^{13}\text{C}$ was 0.19‰, which is higher than in the LGM (mean value of −0.14‰). However, significant decreases of about ~0.31‰ occurred at 3.8–3.1, 5.4–4.9, and 10.5–9 cal kyr BP.

4.2. Radiocarbon Dating of Benthic Foraminifera

^{14}C ages of one planktonic (*G. ruber*) and two benthic (*Cibicoides* spp. and *H. elegans*) foraminiferal species from 11 different sample horizons of core MD 77-176 have been analyzed. Radiocarbon ages for Core MD 77-176 are given in Table 2. ^{14}C ages obtained on benthic *Cibicoides* spp. and *H. elegans* from samples at 65-, 220-, and 400-cm depth give similar ages within the analytical error bar (1 σ ; Table 2). This suggests that correction of age is not useful for the mixed benthic sample (*Cibicoides* spp. and *H. elegans*) analyzed at 558-cm depth. Downcore benthic ^{14}C ages range between 4.18 and 23.55 kyr.

The benthic-planktonic ^{14}C offset (B-P age) is the difference between coexisting benthic and planktonic foraminifera ^{14}C ages. In core MD 77-176, the B-P age offset drops from ~1290 to ~380 years between ~19.6 and 16.9 cal kyr BP (Table 2). The B-P age offset shows a higher value (770 years) around 14 cal kyr BP and then decreases to reach a minimum value of 200 years at 12.3 cal kyr BP. Then, in the upper part of the record, B-P age offset steadily increases to reach a maximum value of ~1210 years over the late Holocene (2.6 cal kyr BP).

4.3. Foraminiferal Assemblages

The diversity of benthic foraminiferal assemblages ranges from 18 to 41 species, with specimen abundance fluctuating between 82 and 648 individuals (supplementary Table S2). The hyaline benthic foraminifera are the dominant constituents (>80%), mainly composed of *Bulimina aculeata*, *H. elegans*, *C. wuellerstorfi*, and *U. peregrina* (in decreasing order of relative average abundance). The mean agglutinated benthic foraminifera relative abundance is only 1.2%, including *Textularia* sp., *Martinottiella communis*, and *Eggerella bradyi*, while the average percentage of porcelaneous forms is about 4.1%, characterized by *Pyrgo lucernula*, *Pyrgo murrhina*, *Pyrgoella osloensis*, *Quinqueloculina* spp., *Sigmoilopsis schlumbergeri*, and *Spiroloculina* spp.

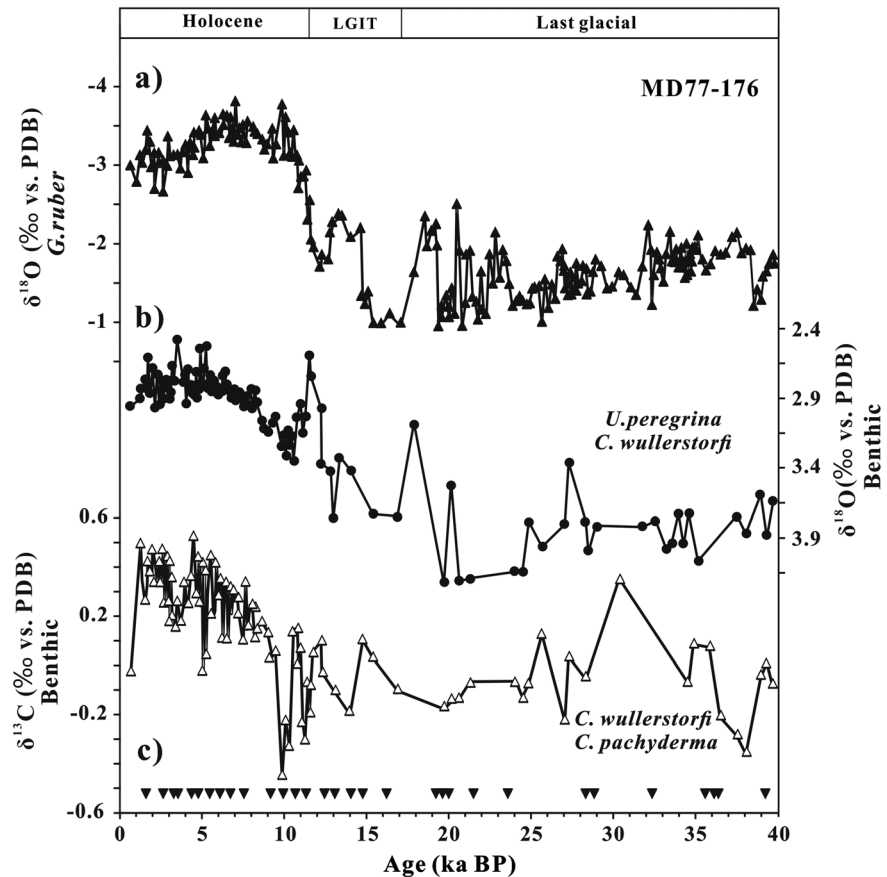


Figure 2. Stable isotopes of oxygen and carbon plotted against age in Core MD77-176. (a) $\delta^{18}\text{O}$ record of the planktonic foraminifera (*G. ruber*, Marzin et al., 2013), (b) benthic $\delta^{18}\text{O}$, and (c) $\delta^{13}\text{C}$ records for MD77-176. The black inverted triangles represent the ^{14}C calculated calendar age points (Marzin et al., 2013). LGIT = last glacial-interglacial transition.

We merged species that show ecological similarities, such as *Globobulimina affinis*, *Globobulimina pacifica*, *Praeglobobulimina spinescens*, and *Praeglobobulimina pupoides*, into *Globobulimina* spp. Species with a relative abundance of >1% in at least one sample were subjected to statistical analysis.

A total of 102 samples and 56 groups/species were selected for principal component analysis (supplementary Table S2). This analysis suggests that benthic foraminiferal faunas can be grouped into two main assemblages that represent about 37% of the total variance (Table 3 and Figure 3). *B. aculeata* and *H. elegans* dominate assemblage 1, which corresponds to the benthic foraminiferal fauna from the late deglaciation to the Holocene (between 14 and 0.7 kyr; Figure 3). The main associated species of assemblage 1 are *C. wullerstorfi* and *Globocassidulina subglobosa*. In contrast, *C. robertsonianus* and *Bolivina robusta* dominate assemblage 2, which is more important during the LGM and the early deglaciation. Other quantitatively important contributors are *C. pachydermus*, *Pullenia bulloides*, and *Globobulimina* spp.

5. Discussion

Results obtained from core MD77-176 reveal (i) a clear glacial-interglacial variability, as already described in the area and at different water depths and (ii) millennial-scale events that punctuated the Last Termination and the Early Holocene. We will discuss the significance of these variations at the core site and also compare the results with records for other water depths in the studied area. Then, we will compare the MD77-176 records with other areas in the ocean, particularly in order to discuss the role of the Southern Ocean in the BoB hydrological variations at intermediate depths.

Table 2
Calibrated AMS ^{14}C Age Determined on Planktonic (Data Taken From Marzin et al., 2013) and Benthic (This Study) Foraminifera Sampled in core MD77-176

Depth (cm)	Calendar age (yr B.P.)	1 sigma error (\pm yr)	Taxa	^{14}C age (year)	1 sigma error (\pm year)	B-P age offsets years	1 sigma error (\pm year)
65	2620	40	<i>G.ruber</i>	3060	60		
65			<i>Cibicoides</i> spp.	4180	60	1120	120
65			<i>Hoeglundina elegans</i>	4270	55	1210	115
220	5520	100	<i>G.ruber</i>	5120	70		
220			<i>Cibicoides</i> spp.	5870	60	750	130
220			<i>Hoeglundina elegans</i>	6110	70	990	140
305	7290	70	<i>G.ruber</i>	6960	80		
305			<i>Hoeglundina elegans</i>	7890	90	930	170
400	9985	180	<i>G.ruber</i>	9350	45		
400			<i>Cibicoides</i> spp.	9730	100	380	145
400			<i>Hoeglundina elegans</i>	9700	90	350	135
445	11000	110	<i>G.ruber</i>	10950	90		
445			<i>Hoeglundina elegans</i>	11080	100	130	190
496	12280	120	<i>G.ruber</i>	11450	90		
496			<i>Hoeglundina elegans</i>	11650	90	200	180
535	14000	230	<i>G.ruber</i>	12910	110		
535			<i>Hoeglundina elegans</i>	13680	110	770	220
565	15405	180	<i>G.ruber</i>	14880	70		
565			<i>Hoeglundina elegans</i>	15260	80	380	150
585	16890	100	<i>G.ruber</i>	16420	70		
585			Mixed two benthic species	17250	280	830	350
617	19580	100	<i>G.ruber</i>	16660	120		
617			<i>Hoeglundina elegans</i>	17950	130	1290	250
740	27060	240	<i>G.ruber</i>	23420	140		
740			<i>Cibicoides</i> spp.	23550	360	130	500

Note. ^{14}C ages were converted into calendar years (cal. yr BP, BP = AD 1950) BY USING THE AGE MODEL ESTABLISHED BY MARZIN ET AL. (2013). SPECIES USED FOR THE RADIOCARBON DATING ARE ALSO REPORTED.

Table 3
Species Composition of Benthic Foraminiferal Assemblages From Core MD77-176

Principal component number	Dominant species		Important associated species	Variance (%)
PC1				37
Negative loadings	<i>Bulimina aculeata</i>	-0.78	<i>Cibicoides wuellerstorfi</i>	-0.05
	<i>Hoeglundina elegans</i>	-0.45	<i>Globocassidulina subglobosa</i>	-0.14
Positive loadings	<i>Cibicoides robertsonianus</i>	0.24	<i>Cibicoides pachyderma</i>	0.1
	<i>Bolivina robusta</i>	0.12	<i>Pullenia bulloides</i>	0.1
			<i>Globobulimina</i> spp.	0.04
PC2				20
Negative loadings	<i>Globocassidulina subglobosa</i>	-0.86	<i>Cibicoides wuellerstorfi</i>	-0.06
	<i>Cibicoides pachyderma</i>	-0.06	<i>Bulimina aculeata</i>	-0.02
Positive loadings	<i>Hoeglundina elegans</i>	0.44	<i>Uvigerina peregrina</i>	0.12
	<i>Bolivina robusta</i>	0.1	<i>Pullenia bulloides</i>	0.03
	<i>Sphaeroidina bulloides</i>	0.09		

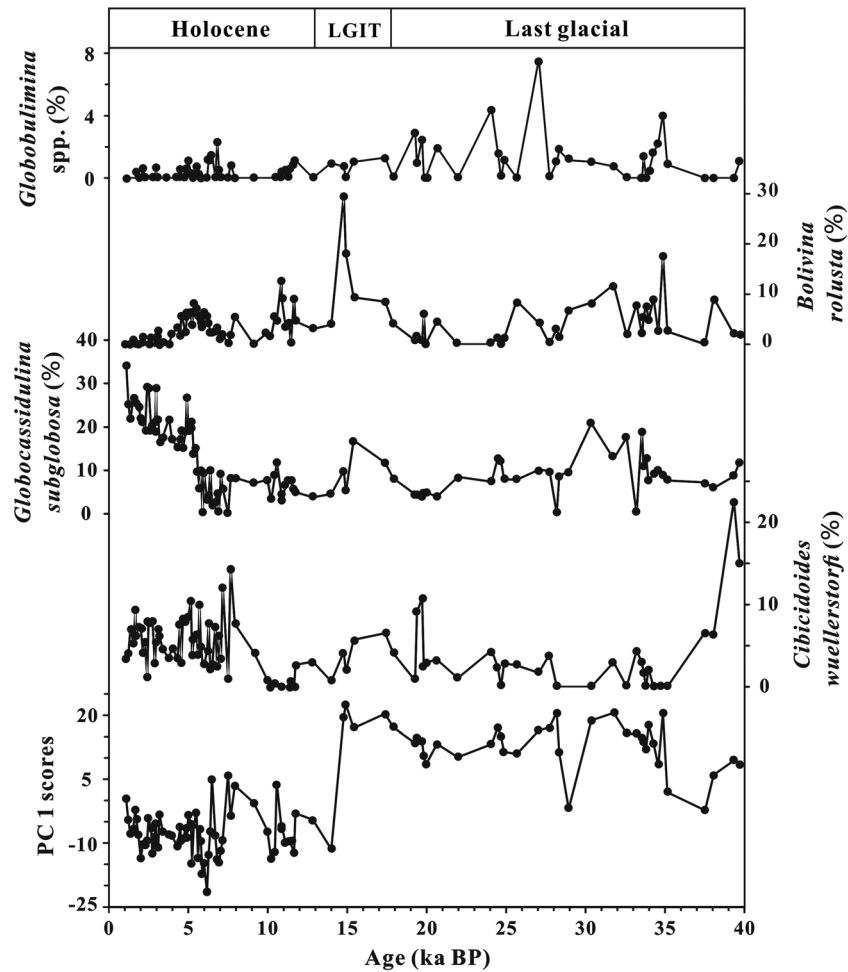


Figure 3. Downcore variations of PC 1 scores and the percentages of major species. LGIT = last glacial-interglacial transition.

5.1. Glacial and Interglacial Variations

Results from core MD77-176 indicate an average value for *Cibicides* $\delta^{13}\text{C}$ of -0.13‰ during the LGM, which is close to the $\delta^{13}\text{C}$ records collected at a deeper water depth, Sk157-14 (3,306 m, $\delta^{13}\text{C}$: -0.05‰), Sk157-15 (2,855 m, $\delta^{13}\text{C}$: -0.11‰), and Sk157-16 (2,920 m, $\delta^{13}\text{C}$: -0.12‰) in the southern BoB (Ahmad et al., 2008; Raza et al., 2014; Figure 1 for core locations) and core RC12344 (2,140 m, -0.12‰) in the Andaman Sea (Naqvi et al., 1994). Glacial to Holocene $\delta^{13}\text{C}$ shift is about 0.35‰ , consistent with previous studies in the northern Indian Ocean (e.g., Curry et al., 1988; Duplessy et al., 1984; Naqvi et al., 1994) and an increased benthic $\delta^{13}\text{C}$ of $0.38 \pm 0.08\text{‰}$ from LGM to Holocene for 0.5–5 km in the global ocean corresponded to the changes in the terrestrial carbon reservoir (Peterson et al., 2014). This increase from the LGM to the Holocene reflects more invigorated circulation associated with better ventilated waters at intermediate depth in the Northern BoB during the Holocene (Duplessy et al., 1984; Waelbroeck et al., 2006).

During the LGM, the outflow from the Red Sea, Persian Gulf, and the ITF was greatly reduced, or ceased altogether, due to sea-level lowstand (Locke & Thunell, 1988; Naqvi et al., 1994; Siddall et al., 2003). Lower values of $\delta^{13}\text{C}$ during the LGM in the BoB have been interpreted as reflecting a reduction in the NADW flux into the southern BoB, and an increased contribution from the SSW (Ahmad et al., 2008, 2012; Raza et al., 2014). Such results are also consistent with the radiogenic ϵ_{Nd} values (from -6.5 to -8) observed on several cores collected at different water depths of the BoB which indicate a higher contribution of SSW before 18 cal kyr BP (Figure 4; Yu et al., 2018).

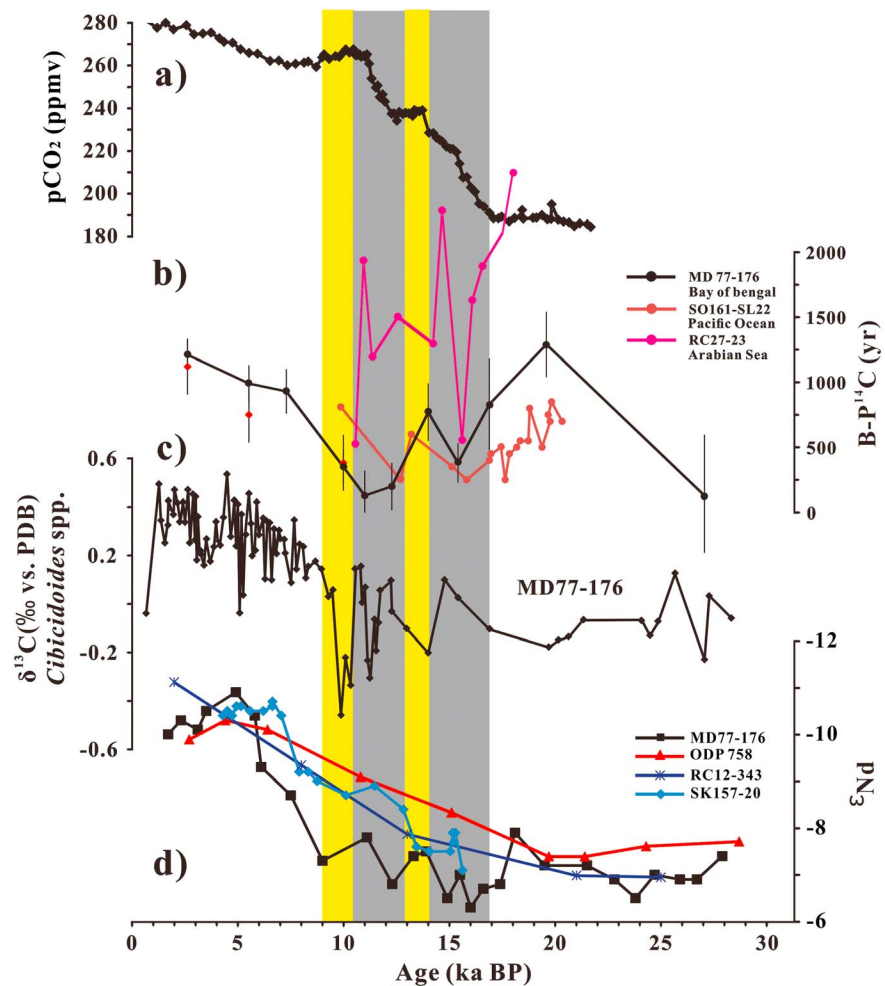


Figure 4. (a) Ice core atmospheric CO₂ from Antarctic Dome C (Monnin et al., 2001), (b) comparison of the intermediate water B-P ¹⁴C age offset: Arabian Sea records, shown in pink (RC 27-23; Bryan et al., 2010), dark red (SO161-SL22; De Pol-Holz et al., 2010) and MD 77-176 (black, B-P ¹⁴C age offset calculated by benthic *H. elegans* age, red diamond, calculated by benthic *Cibicoides* spp.), (c) benthic δ¹³C records for MD77-176, (d) comparison of seawater ε_{Nd} records in BoB obtained from planktonic foraminifera in core MD77-176 (Yu et al., 2018), core RC12-343 (Stoll et al., 2007), SK157-20 (Naik et al., 2019), and ODP site 758 (Burton & Vance, 2000). The gray-shaded intervals mark the two-step increase in atmospheric CO₂; the yellow-shaded interval marks the 14–13 cal kyr BP interval and the early Holocene (10.5–9 cal kyr BP), respectively.

This is also supported by a δ¹⁸O shift of 1.8‰ from the LGM to the Holocene in core MD 77-176, in agreement with other benthic δ¹⁸O records from the BoB (Ahmad et al., 2008, 2012; Naqvi et al., 1994; Raza et al., 2014). If we assume a limited deep local salinity change at the studied site during the LGM, and an ice-volume effect of about 1 to 1.2‰, the higher values of benthic δ¹⁸O during the LGM indicate that temperature of the intermediate water in the northern BoB was about 3–4 °C lower than those of the Holocene. Such colder intermediate water in the BoB can be linked to a higher proportion of cold deep water masses.

The δ¹³C and δ¹⁸O records obtained on benthic foraminifera and the foraminiferal ε_{Nd} record accord closely with the faunal record, which is dominated during the LGM by assemblage 2 (Figure 3 and Figure S1), of which *B. robusta*, *P. bulloides* and *Globobulimina* spp. are major components. The distribution of living *B. robusta* ranges from 700 to 2,000 m and is associated with low dissolved oxygen conditions (Murgese & De Deckker, 2007; Szarek et al., 2009). *P. bulloides* and *Globobulimina* spp. prefer an intermediate to deep infaunal microhabitat, associated with a meso-eutrophic environment in poorly ventilated deep waters (e.g., Corliss, 1985; Fontanier et al., 2002). Thus, assemblage 2 could indicate relatively low-oxygen and mesotrophic to eutrophic bottom water conditions during the LGM. This environment may be linked to the higher

contribution of the SSW, which is known to present a higher trophic condition and a lower oxygen concentration than waters from the North Atlantic.

By contrast, assemblage 1 dominates during the Holocene. The major species are *B. aculeata*, *H. elegans*, *C. wuellerstorfi*, and *G. subglobosa*. Previous studies on *B. aculeata* indicate that this species has a widespread distribution and shows adaptability with respect to food (e.g., Altenbach et al., 1999; Cauille et al., 2015). However, *H. elegans*, *C. wuellerstorfi*, and *G. subglobosa* were observed in areas with low organic carbon flux rates and in high-oxygen content water masses (e.g., Altenbach et al., 1999; De & Gupta, 2010; Fontanier et al., 2002, and references therein). Periods dominated by these taxa probably correspond to high oxygen levels and oligotrophic environments. All of those elements suggest that intermediate water masses during the Holocene were characterized by oligotrophic to mesotrophic conditions and/or well-ventilated conditions.

Today, the deep water in the BoB is filled with a mixture of NADW and Circumpolar Deep Water (Talley et al., 2011). In the northern BoB, the bottom water could contribute to shallower-depth water masses, because bottom water can upwell when it flows northward (Naqvi et al., 1994; Talley et al., 2011). The Glacial to Holocene *Cibicidoides* $\delta^{13}\text{C}$ shift is around 0.35‰ at core MD77-176 site, consistent with the average $\delta^{13}\text{C}$ shift ($\sim 0.4\text{‰}$) obtained from RC12-344 (2,140 m, intermediate water depth) in the Andaman Sea (Naqvi et al., 1994). However, at deeper water depth from the southern BoB (Sk157-14, 3,306 m; Sk157-15, 2,855 m; Sk157-16, 2,920 m), the average Glacial to Holocene *Cibicidoides* $\delta^{13}\text{C}$ shift is around 0.6‰–0.65‰. This benthic $\delta^{13}\text{C}$ shift is interpreted as reflecting the enhanced influence of better-ventilated deep water NADW (Ahmad et al., 2008; Raza et al., 2014). Thus, the increased benthic $\delta^{13}\text{C}$ at intermediate water at the studied site may also reflect the enhanced contribution of NADW during the Holocene. Compared with deeper records of *Cibicidoides* $\delta^{13}\text{C}$, the benthic $\delta^{13}\text{C}$ at intermediate water depth may also be affected by the larger river input during the Holocene (Marzin et al., 2013), discharging lighter ^{13}C terrigenous organic matter into the ocean margin. However, in the modern situation, the percentage of terrigenous organic carbon from the Irrawaddy River decreases gradually offshore. On the outer Irrawaddy continental shelf, the contribution of terrigenous organic carbon is reduced and does not seem to a large contribution at the core site (Ramaswamy et al., 2008). In addition, benthic foraminifera assemblage 1 is also consistent with the higher values of *Cibicidoides* $\delta^{13}\text{C}$, reflecting better-ventilated waters at the core site during the Holocene that could correspond to NADW. Thus, we suggest that benthic $\delta^{13}\text{C}$ during the Holocene is mainly influenced by the better-ventilated water masses (NADW).

In addition, B-P ^{14}C values dramatically increase from 10 cal kyr BP onward, and reach a maximum ($\sim 1,210$ years) at 2.6 cal kyr BP (late Holocene). The maximum value in the late Holocene is similar to the B-P age offset of $\sim 1,290$ years at 19.6 cal kyr BP (during the LGM; Figure 4). Higher values of B-P age offset could indicate intrusions of deep old water masses and a strong stratification of the upper water column. Moreover, the decrease in ϵ_{Nd} at deep water depth of the BoB could be interpreted as the increased influence of NADW (-13), and/or enhanced nonradiogenic Nd inputs from Ganges-Brahmaputra river system during the Holocene (Naik et al., 2019; Yu et al., 2018). Combined with the $\delta^{13}\text{C}$, $\delta^{18}\text{O}$ and assemblage records, higher values of B-P ^{14}C age offset may also suggest the contribution of NADW and SSW, respectively, during the late Holocene and LGM.

Our results indicate that during the LGM, deep and intermediate waters in the BoB were dominated by SSW, with a lesser contribution of water mass from the North Atlantic Ocean; this is in contrast to the Holocene. Bottom conditions changed from eutrophic to oligotrophic as we move from the LGM toward the Holocene, which could indicate a reduction in the supply of organic matter and an increase in oxygen levels in the bottom water.

5.2. Millennial-Scale Variations

5.2.1. Intermediate and Deep Water Depth Evolution in the BoB during the Last Termination and the Early Holocene

Superimposed on the glacial-interglacial trends, short events have also been recorded at the Core MD77-176 site during the 17–14, 13–10.6, and 10.5–9 cal kyr BP intervals. Increases of $\delta^{13}\text{C}$ values in the 17–14 and 13–10.6 cal kyr BP intervals correspond to reductions of B-P ^{14}C age offset to around ~ 300 and 200 years, respectively (Figure 4). The $\delta^{13}\text{C}$ decreases at around 10.5–9 cal kyr BP are coeval with lower values of B-P ^{14}C age offset of about ~ 350 years. The B-P ^{14}C age offsets subsequently increase significantly from 10 kyr onward

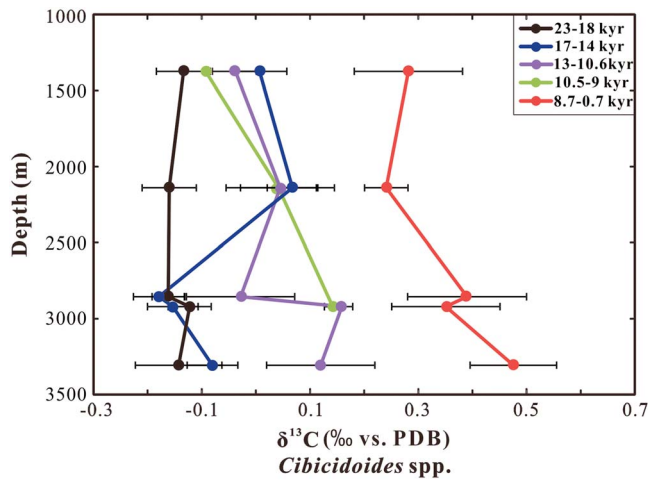


Figure 5. Benthic average $\delta^{13}\text{C}$ profiles for each of the cores in the vertical transects for selected time slices (23–18, 17–14, 13–10.6, 10.5–9, and 8.7–0.7 cal kyr BP). The $\delta^{13}\text{C}$ data are obtained from Sk157-14 (3,306 m), Sk157-15 (2,855 m), and Sk157-16 (2,920 m) in the southern BoB (Ahmad et al., 2008; Raza et al., 2014) and core RC12-344 (2,140 m) in the Andaman Sea (Naqvi et al., 1994).

and reach a maximum value of $\sim 1,210$ years at the late Holocene (2.6 kyr). In addition, even if the benthic $\delta^{18}\text{O}$ record does not exhibit a clear trend during the 17–14 cal kyr BP interval, a significant decrease in values of about 2.5‰ – 3‰ occurred at 13–10.6 cal kyr BP (Figure 2).

In order to examine the changes on a millennial time-scale during the last deglaciation and early Holocene at intermediate and deep water depth in the BoB, we compared the benthic $\delta^{13}\text{C}$ record of MD77-176 with the $\delta^{13}\text{C}$ record at intermediate depth from the Andaman Sea (RC12-344, 12.46°N – 96.04°E , 2,140-m water depth; Naqvi et al., 1994), and at deep water depth from the southern BoB (Sk157-14, $5^\circ11'\text{N}$ – $90^\circ05'\text{E}$, 3,306 m; Sk157-15, $7^\circ48'\text{N}$ – $90^\circ15'\text{E}$, 2,855 m; Sk157-16, $8^\circ46'\text{N}$ – $90^\circ18'\text{E}$, 2,920 m; Ahmad et al., 2008; Raza et al., 2014). We averaged the benthic $\delta^{13}\text{C}$ of each core in different time intervals (23–18, 17–14, 13–10.6, 10.5–9, and 8.7–0.7 cal kyr BP) and plotted the results as vertical depth profiles (Figure 5). During the LGM, benthic $\delta^{13}\text{C}$ records obtained at intermediate and deep depths show similar values ($\sim -0.15\text{‰}$). Then, the $\delta^{13}\text{C}$ records show a continuous increase throughout the deglaciation until the Holocene. However, the evolution of deep and intermediate water mass $\delta^{13}\text{C}$ is quite different over the intervals 17–14, 13–10.6, and 10.5–9 cal kyr BP. After 23–18 cal kyr BP, the intermediate $\delta^{13}\text{C}$ values display an increasing trend at 17–14 and 13–10.6 cal kyr BP intervals, while during the 17–14 cal kyr

BP interval the $\delta^{13}\text{C}$ records from deep water depths show similar $\delta^{13}\text{C}$ values to those of the LGM and they begin to increase from the 13–10.6 cal kyr BP interval onward. This difference suggests an increased stratification between intermediate and deeper water masses during the last deglaciation. In addition, the $\delta^{13}\text{C}$ decrease around 10.5–9 cal kyr BP (early Holocene) is also observed in the deep water depth cores from the southern BoB (Ahmad et al., 2008; Raza et al., 2014), with a clear shift from the early Holocene to late Holocene.

The last glacial period and the last deglaciation, until approximately 10.5 cal kyr, were characterized by ϵ_{Nd} values of between -7.9 ± 0.3 and -6.3 ± 0.2 in core MD77-176 (Figure 4). Before 18 cal kyr BP, the ϵ_{Nd} values of intermediate and deep-water masses are quite similar and become decoupled during the deglaciation. From 18 to 9 kyr BP, the ϵ_{Nd} values of deep water display a decreasing trend dropping down to ~ -9 . However, the ϵ_{Nd} record obtained on intermediate-depth core MD77-176 maintains an increasing trend at 17–14, 13–10.6, and 10.5–9 cal kyr BP intervals (ϵ_{Nd} values range between -8 and -6). The decoupling of ϵ_{Nd} values between various water depths since the LGM may reflect enhanced stratification between deep and intermediate water during the deglacial period (Yu et al., 2018). This is in agreement with the evolution of the vertical profile of *Cibicidoides* $\delta^{13}\text{C}$ collected from different water depth cores in the BoB (Figure 5). The deeper water masses could be associated with a higher contribution of unradiogenic NADW ϵ_{Nd} values from about 18 cal kyr BP, whereas intermediate water masses are associated with a higher contribution of AAIW implying a strong propagation of SSW (AAIW) into the Northern Indian Ocean (Yu et al., 2018).

However, changes in $\delta^{13}\text{C}$ values of benthic foraminifera can be influenced by different processes such as surface productivity, changes of the water mass sources and/or mixing and air-sea exchanges (Lynch-Stieglitz et al., 1995). The B-P ^{14}C age offset could also reflect the source of water masses and/or the renewal process of deep water masses. Therefore, we will discuss these issues in greater detail below and will combine our data to enable us to decipher these different processes.

5.2.2. Variations in Local Processes

Variations of primary productivity can impact the $\delta^{13}\text{C}$ of benthic foraminifera, but do not appear to be a major control at our core site. The distribution of chlorophyll in surface water of the western BoB suggests a slight increase in productivity during the winter monsoon period (around January) in the BoB (O'Malley, 2017; Thushara & Vinayachandran, 2016). The Indian summer monsoon intensity decreased, relatively speaking, during the 17–14 and 13–10.6 cal kyr BP intervals (Marzin et al., 2013), whereas East Asia Winter Monsoon (EAWM) strengthened during the same intervals (Wen et al., 2016). If the intensity of EAWM influenced our core site in the BoB during the 17–14 and 13–10.6 cal kyr BP intervals, we should

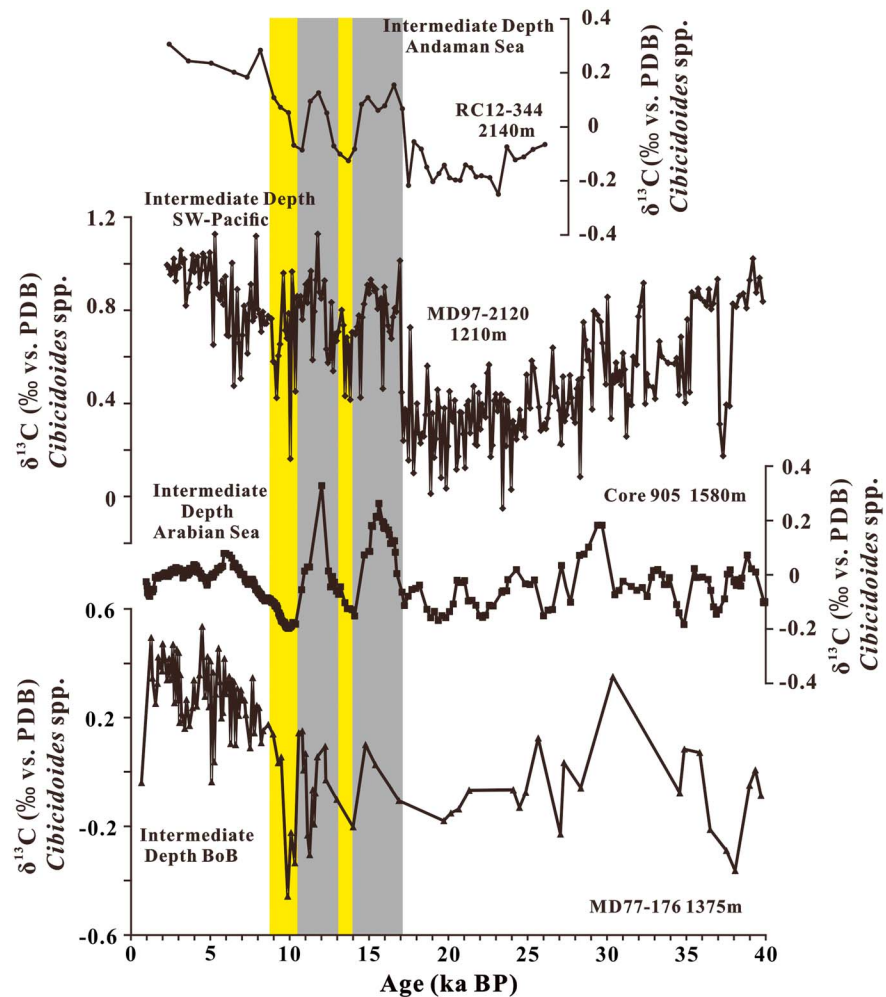


Figure 6. Compilation of benthic $\delta^{13}\text{C}$ records obtained from core MD77-176 (water depth of 1,325-m; this study), core RC12-344 (2,140-m water depth; Naqvi et al., 1994), MD97-2120 (1,210-m water depth; Pahnke & Zahn, 2005), and core 905 (1,580-m water depth; Jung et al., 2009). The color-shaded intervals are the same as in Figure 4.

expect an increased surface productivity during those intervals of intense winter monsoon and, therefore, lower *Cibicides* $\delta^{13}\text{C}$ values through enhanced export and decay of organic carbon at intermediate depth. This is in contradiction to what we observe in the $\delta^{13}\text{C}$ record of MD77-176. Thus, the influence of primary productivity on the benthic $\delta^{13}\text{C}$ values can be discounted.

The *G. ruber* $\delta^{18}\text{O}$ record of core MD77-176 indicates the surface salinity variations in the core site (Marzin et al., 2013), and the lower salinity during the earliest Holocene (around 10 kyr) is associated with an intensified Indian monsoon, leading to more freshwater discharge from the Ganges-Brahmaputra river system and from the Irrawaddy River. This should have led to pronounced ocean stratification of the northern BoB. During this period, however, we observe a decrease in the B-P age offsets, the opposite of what would be expected from strong upper water column stratification. Thus, we suggest that vertical mixing does not appear to play an important role in this area.

5.2.3. Changes in Intermediate Water Circulation

We compared the benthic $\delta^{13}\text{C}$ record of MD77-176 with $\delta^{13}\text{C}$ records at intermediate depth from the Arabian Sea (Core 905, $10^{\circ}46'\text{N}$ – $51^{\circ}57'\text{E}$, 1,580-m water depth), the Southwest Pacific Ocean (MD97-2120, $45^{\circ}32.06'\text{S}$ – $174^{\circ}55.85'\text{E}$, 1,210-m water depth) and the Andaman Sea (RC12-344, 12.46°N – 96.04°E , 2,140-m water depth; Jung et al., 2009; Naqvi et al., 1994; Pahnke & Zahn, 2005; Figure 6). All of the benthic $\delta^{13}\text{C}$ records display an increasing trend during the 17–14 cal kyr BP and 13–10.6 cal kyr BP intervals. Furthermore, we also observed a decrease in those intermediate $\delta^{13}\text{C}$ records at the beginning of the

Holocene (10.5–9 cal kyr BP; Jung et al., 2009; Naqvi et al., 1994; Pahnke & Zahn, 2005; Figure 6). This suggests that the variations during these intervals are related to global changes at intermediate water depths in the Indo-Pacific region. The similarity of the benthic $\delta^{13}\text{C}$ -increases reflects the northward expansion of AAIW during these time intervals in the Arabian Sea and Pacific Ocean (Jung et al., 2009; Pahnke & Zahn, 2005). In addition, the transition in the ϵ_{Nd} and $\Delta^{14}\text{C}$ records during the deglaciation also indicates a strong northward penetration of AAIW within the North Atlantic (e.g., Cao et al., 2007; Pahnke et al., 2008). Combined with the ϵ_{Nd} record of core MD77-176, all of these signals tend to show that, during 17–14 cal kyr BP and 13–10.6 cal kyr BP intervals, BoB circulation was driven by Southern Ocean processes.

By contrast, the generally decreased trend in the presented intermediate benthic $\delta^{13}\text{C}$ records during the 14–13 cal kyr BP interval associated to a more stable ϵ_{Nd} may indicate the weakened formation and northward advection of AAIW (Yu et al., 2018). In addition, the decrease of intermediate benthic $\delta^{13}\text{C}$ corresponds to the rapid increase in sea-level during the ~14–14.5 cal kyr BP time interval, the so-called Melt-Water Pulse 1A (MWP-1A; Deschamps et al., 2012; Fairbanks et al., 2005; Peltier & Fairbanks, 2006). This significant sea-level fluctuation during the 14–13 cal kyr BP interval could have influenced the discharge of terrigenous organic matter into the ocean. Thus, this large input of lighter $\delta^{13}\text{C}$ terrigenous organic carbon may have contributed to the global decrease in the benthic foraminifer $\delta^{13}\text{C}$ values.

The changes in the carbon isotope record and B-P age offsets obtained on the sedimentary section from MD77-176 at the 17–14 and 13–10.6 cal kyr BP intervals correspond to warming episodes in Antarctica and the Southern Hemisphere during the deglaciation (e.g., Cuffey et al., 2016; Epica, 2006). These time intervals also correspond to a decrease of the Antarctic sea-ice (Shemesh et al., 2002; Wais, 2013) and the reduction of stratification resulting in better ventilation in the South Ocean (e.g., Anderson et al., 2009; Skinner et al., 2010). The Southern Hemisphere westerlies migrated to a southern position during those same intervals, which could have led to an increase of the northward Ekman transport (Toggweiler et al., 2006). Therefore, during the 17–14 and 13–10.6 cal kyr BP intervals, enhanced vertical ventilation in the Southern Ocean could have led to an increased production of subsurface water masses (Subantarctic Mode Water, SAMW) and intermediate water masses (AAIW; Anderson et al., 2009). These water masses could have carried a chemical signature resulting in a reduced difference between intermediate and surface water masses (e.g., $\delta^{13}\text{C}$ values, B-P offsets, temperature, and salinity) and which was transported at the same time to the north.

Strengthened upward mixing would provide a conduit for moving much younger ^{14}C age surface water to deep water masses; this in turn may lead to a greater decrease of the B-P age offsets. In addition, the intermediate benthic $\delta^{13}\text{C}$ in the Southern Ocean is dominated by the influence of air-sea exchange (Lynch-Stieglitz et al., 1994), and values of intermediate benthic $\delta^{13}\text{C}$ could increase relatively via stronger upwelling during the formation of AAIW/SAMW. Such a hypothesis is consistent with the variations of intermediate benthic $\delta^{13}\text{C}$ records and B-P age offsets from the Northern BoB, Arabian Sea, and Pacific Ocean (Figures 6 and 4b). Coinciding with the carbon isotopes and ^{14}C ages, the disconnection observed in the ϵ_{Nd} values between core MD77-176 and the other deeper cores of the BoB during the deglaciation could confirm the influence of glacial radiogenic AAIW (Yu et al., 2018; Figure 4d).

Increased benthic carbon isotope values and smaller B-P age offsets obtained from MD77-176 at 17–14 and 13–10.6 cal kyr BP intervals are synchronous with a two-step increase of atmospheric CO_2 (Figure 4). The changes in B-P age offset and benthic $\delta^{13}\text{C}$ records reported here indicate strong upwelling and enhanced northern flow of AAIW from the Southern Ocean during these two periods. Thus, the variations of these records could support the hypothesis that the Southern Ocean upwelling played a vital role for the CO_2 increase in the deglacial period (Anderson et al., 2009; Skinner et al., 2010; Skinner et al., 2014).

The variations of intermediate benthic $\delta^{13}\text{C}$, B-P age offsets and ϵ_{Nd} records during the 17–14 and 13–10.6 cal kyr BP intervals correspond to warming in South Hemisphere and increased atmospheric CO_2 . These elements support the idea of more fresh water input in the North Atlantic Ocean and associated to a weakened northward transport of heat. Synchronously, the Southern Hemisphere increased the heat fluxes and reduced sea ice cover in the Southern Ocean. Thus, strong winds enhanced the upwelling and increased the northward penetration of the northward flow of AAIW/SAMW, which could increase northward transport of nutrient and heat at intermediate waters depth (Anderson et al., 2009; Poggemann et al., 2017, 2018;

Skinner et al., 2014). The role of AAIW is still controversial during the last deglaciation in the Atlantic Ocean, several studies suggesting a reduced northward flux of AAIW into the tropical Atlantic (e.g., Came et al., 2008; Gu et al., 2017; Howe et al., 2016; Xie et al., 2012). However, other studies indicate an increased penetration of AAIW in the Atlantic Ocean (e.g., Dubois-Dauphin et al., 2016; Pahnke et al., 2008; Poggemann et al., 2017, 2018). This is also strongly supported by the intermediate records of benthic carbon isotope, ϵ_{Nd} , and B-P age offsets from the North Indian (Bryan et al., 2010; Jung et al., 2009; Yu et al., 2018), and Pacific Ocean (e.g., Bostock et al., 2010; Mix et al., 1991; Pahnke & Zahn, 2005). Therefore, we suggest that the global northern flow intermediate water was sourced from the Southern Ocean by AAIW/SAMW during the deglaciation.

$\delta^{13}\text{C}$ records subsequently display a short-term decreasing trend in the northern Indian Ocean and SW Pacific Ocean at the beginning of the Holocene (10.5–9 cal kyr BP; Jung et al., 2009; Naqvi et al., 1994; Pahnke & Zahn, 2005). The B-P ^{14}C age offsets and ϵ_{Nd} from core MD77-176 are close to the values obtained for the deglaciation (Figure 4). Thereafter, from the 10.5–9 cal kyr BP interval to the late Holocene, the increased benthic $\delta^{13}\text{C}$ and B-P age offsets, associated to depleted ϵ_{Nd} records, seem to indicate the enhanced influence of the NADW since the 9 cal kyr BP. Thus, we suggest that the BoB circulation during the 10.5–9 cal kyr BP interval was also driven by the northward expansion of AAIW, with a progressive increase in the influence of the NADW during the Holocene, as is also indicated by the $\delta^{18}\text{O}$ and benthic assemblage records.

6. Conclusions

Changes in benthic foraminiferal assemblages, together with $\delta^{13}\text{C}$, $\delta^{18}\text{O}$, and ^{14}C ages obtained from benthic foraminifera have been analyzed on core MD77-176, located in the BoB at 1,375-m water depth, in order to reconstruct the evolution of intermediate water masses in the northeast Indian Ocean from the LGM to the Holocene. Benthic $\delta^{13}\text{C}$ and $\delta^{18}\text{O}$ records suggest that the LGM was dominated by expansion of South Ocean waters with low $\delta^{13}\text{C}$ values, whereas the late Holocene is characterized by strengthened NADW flows into the BoB, with higher values of $\delta^{13}\text{C}$ and B-P age offsets. Benthic foraminiferal assemblages are consistent with the geochemical proxies, with the LGM assemblage reflecting a relatively low-oxygen level and mesotrophic to eutrophic deep water conditions. The typically Holocene assemblage indicates well-ventilated conditions and/or an oligotrophic to mesotrophic environment.

Furthermore, during the last deglaciation to the Early Holocene, events at 17–14, 13–10.6, and 10.5–9 cal kyr BP intervals display decreased B-P age offsets, increased benthic $\delta^{13}\text{C}$ records, and changes in the $\delta^{18}\text{O}$ values and ϵ_{Nd} results. All of these results are best explained by a northern Indian Ocean variation associated with changes in water masses formed in the South. Our proxy variations are consistent with enhanced upwelling in the Southern Ocean and increased northward penetration of the northward flow of AAIW/SAMW during the 17–14, 13–10.6, and 10.5–9 cal kyr BP intervals. These signals are coeval with the two-step increase of atmospheric carbon dioxide (CO_2), indicating that the enhanced Southern Ocean ventilation could have played an important role in the CO_2 increase during the last deglaciation.

Acknowledgments

This work was supported by the National Natural Science Foundation of China (41806060). R. Ma acknowledges the China Scholarship Council for providing funding for her study in France. We thank F. Thil for the ^{14}C measurements taken using the ECHOMICADAS and two anonymous reviewers for useful suggestions and discussions. This work has been supported by grants from the INSU-LEFE-IMAGO-CITRON GLACE program. All data are given in Tables 1–3 and S1 and S2.

References

- Ahmad, S. M., Babu, A. G., Padmakumari, V. M., & Raza, W. (2008). Surface and deep water changes in the northeast Indian Ocean during the last 60 ka inferred from carbon and oxygen isotopes of planktonic and benthic foraminifera. *Palaeogeography, Palaeoclimatology, Palaeoecology*, 262(3–4), 182–188. <https://doi.org/10.1016/j.palaeo.2008.03.007>
- Ahmad, S. M., Zheng, H., Raza, W., Zhou, B., Lone, M. A., Raza, T., & Suseela, G. (2012). Glacial to Holocene changes in the surface and deep waters of the Northeast Indian Ocean. *Marine Geology*, 329–331, 16–23. <https://doi.org/10.1016/j.margeo.2012.10.002>
- Altenbach, A. V., Pflaumann, U., Thies, R. S. A., Timm, S., & Trauth, M. (1999). Scaling percentages and distributional patterns of benthic foraminifera with flux rates of organic carbon. *Journal of Foraminiferal Research*, 29(3), 173–185.
- Anderson, R. F., Ali, S., Bradtmiller, L. I., Nielsen, S. H. H., Fleisher, M. Q., Anderson, B. E., & Burckle, L. H. (2009). Wind-driven upwelling in the Southern Ocean and the deglacial rise in atmospheric CO_2 . *Science*, 323(5920), 1443–1448. <https://doi.org/10.1126/science.1167441>
- Böhm, E., Lippold, J., Gutjahr, M., Frank, M., Blaser, P., Antz, B., et al. (2015). Strong and deep Atlantic meridional overturning circulation during the last glacial cycle. *Nature*, 517(7532), 73–76. <https://doi.org/10.1038/nature14059>
- Bostock, H. C., Opydyke, B. N., & Williams, M. J. M. (2010). Characterising the intermediate depth waters of the Pacific Ocean using $\delta^{13}\text{C}$ and other geochemical tracers. *Deep Sea Research Part I: Oceanographic Research Papers*, 57(7), 847–859. <https://doi.org/10.1016/j.dsr.2010.04.005>
- Bryan, S. P., Marchitto, T. M., & Lehman, S. J. (2010). The release of ^{14}C -depleted carbon from the deep ocean during the last deglaciation: Evidence from the Arabian Sea. *Earth and Planetary Science Letters*, 298(1–2), 244–254. <https://doi.org/10.1016/j.epsl.2010.08.025>

- Burton, K. W., & Vance, D. (2000). Glacial–interglacial variations in the neodymium isotope composition of seawater in the Bay of Bengal recorded by planktonic foraminifera. *Earth and Planetary Science Letters*, *176*(3–4), 425–441. [https://doi.org/10.1016/S0012-821X\(00\)00011-X](https://doi.org/10.1016/S0012-821X(00)00011-X)
- Came, R. E., Oppo, D. W., Curry, W. B., & Lynch-Stieglitz, J. (2008). Deglacial variability in the surface return flow of the Atlantic meridional overturning circulation. *Paleoceanography*, *23*, PA1217. <https://doi.org/10.1029/2007PA001450>
- Cao, L., Fairbanks, R., Mortlock, R., & Risk, M. (2007). Radiocarbon reservoir age of high latitude North Atlantic surface water during the last deglacial. *Quaternary Science Reviews*, *26*(5–6), 732–742. <https://doi.org/10.1016/j.quascirev.2006.10.001>
- Caulle, C., Mojtabid, M., Gooday, A. J., Jorissen, F. J., & Kitazato, H. (2015). Living (Rose-Bengal-stained) benthic foraminiferal faunas along a strong bottom-water oxygen gradient on the Indian margin (Arabian Sea). *Biogeosciences*, *12*(16), 5005–5019. <https://doi.org/10.5194/bg-12-5005-2015>
- Corliss, B. H. (1985). Microhabitats of benthic foraminifera within deep-sea sediments. *Nature*, *314*(6010), 435–438. <https://doi.org/10.1038/314435a0>
- Cuffey, K. M., Clow, G. D., Steig, E. J., Buizert, C., Fudge, T. J., Koutnik, M., et al. (2016). Deglacial temperature history of West Antarctica. *Proceedings of the National Academy of Sciences*, *113*(50), 14,249–14,254. <https://doi.org/10.1073/pnas.1609132113>
- Curry, W. B., Duplessy, J. C., Labeyrie, L. D., & Shackleton, N. J. (1988). Changes in the distribution of $\delta^{13}\text{C}$ of deep water ΣCO_2 between the Last Glaciation and the Holocene. *Paleoceanography*, *3*(3), 317–341. <https://doi.org/10.1029/PA003i003p00317>
- De Pol-Holz, R., Keigwin, L., Southon, J., Hebbeln, D., & Mohtadi, M. (2010). No signature of abyssal carbon in intermediate waters off Chile during deglaciation. *Nature Geoscience*, *3*(3), 192–195. <https://doi.org/10.1038/ngeo745>
- De, S., & Gupta, A. K. (2010). Deep-sea faunal provinces and their inferred environments in the Indian Ocean based on distribution of recent benthic foraminifera. *Palaeogeography, Palaeoclimatology, Palaeoecology*, *291*(3–4), 429–442. <https://doi.org/10.1016/j.palaeo.2010.03.012>
- Deschamps, P., Durand, N., Bard, E., Hamelin, B., Camoin, G., Thomas, A. L., et al. (2012). Ice-sheet collapse and sea-level rise at the Bølling warming 14,600 years ago. *Nature*, *483*(7391), 559–564. <https://doi.org/10.1038/nature10902>
- Dubois-Dauphin, Q., Bonneau, L., Colin, C., Montero-Serrano, J. C., Montagna, P., Blamart, D., et al. (2016). South Atlantic Intermediate Water advances into the north-east Atlantic with reduced Atlantic meridional overturning circulation during the last glacial period. *Geochemistry, Geophysics, Geosystems*, *17*, 2336–2353. <https://doi.org/10.1002/2016GC006281>
- Duplessy, J. C., Shackleton, N. J., Matthews, R. K., Prell, W., Ruddiman, W. F., Caralp, M., & Hendy, C. H. (1984). ^{13}C record of benthic foraminifera in the last interglacial ocean: Implications for the carbon cycle and the global deep water circulation. *Quaternary Research*, *21*(02), 225–243. [https://doi.org/10.1016/0033-5894\(84\)90099-1](https://doi.org/10.1016/0033-5894(84)90099-1)
- EPICA, C.M (2006). One-to-one coupling of glacial climate variability in Greenland and Antarctica. *Nature*, *444*(7116), 195–198. <https://doi.org/10.1038/nature05301>
- Fairbanks, R. G., Mortlock, R. A., Chiu, T.-Z., Cao, L., Kaplan, A., Guilderson, T. P., et al. (2005). Radiocarbon calibration curve spanning 0 to 50,000 years BP based on paired $^{230}\text{Th}/^{234}\text{U}/^{238}\text{U}$ and ^{14}C dates on pristine corals. *Quaternary Science Reviews*, *24*(16–17), 1781–1796. <https://doi.org/10.1016/j.quascirev.2005.04.007>
- Fontanier, C., Jorissen, F. J., Licari, L., Alexandre, A., Anschutz, P., & Carbonel, P. (2002). Live benthic foraminiferal faunas from the Bay of Biscay: Faunal density, composition, and microhabitats. *Deep Sea Research Part I: Oceanographic Research Papers*, *49*(4), 751–785. [https://doi.org/10.1016/S0967-0637\(01\)00078-4](https://doi.org/10.1016/S0967-0637(01)00078-4)
- Gu, S., Liu, Z., Zhang, J., Rempfer, J., Joos, F., & Oppo, D. W. (2017). Coherent response of Antarctic Intermediate Water and Atlantic Meridional Overturning during the last deglaciation: Reconciling contrasting neodymium isotope reconstructions from the tropical Atlantic. *Paleoceanography*, *32*, 1036–1053. <https://doi.org/10.1002/2017PA003092>
- Hammer, Ø., Harper, D.A.T., and Ryan, P.D. (2001). Past: Paleontological statistics software package for education and data analysis. Holbourn, A., Henderson, A. S., & Macleod, N. (2013). Front matter. In *Atlas of benthic foraminifera*, (pp. 1–641).
- Howe, J. N. W., Piotrowski, A. M., Oppo, D. W., Huang, K. F., Mulitza, S., Chiessi, C. M., & Blusztajn, J. (2016). Antarctic intermediate water circulation in the South Atlantic over the past 25,000 years. *Paleoceanography*, *31*, 1302–1314. <https://doi.org/10.1002/2016PA002975>
- Jones, R. W. (1994). *The challenger foraminifera*, (p. 149). Oxford University Press.
- Jung, S. J. A., Kroon, D., Ganssen, G., Peeters, F., & Ganeshram, R. (2009). Enhanced Arabian Sea intermediate water flow during glacial North Atlantic cold phases. *Earth and Planetary Science Letters*, *280*(1–4), 220–228. <https://doi.org/10.1016/j.epsl.2009.01.037>
- Kallel, N., Labeyrie, L. D., Juillet-Leclerc, A., & Duplessy, J. C. (1988). A deep hydrological front between intermediate and deep-water masses in the glacial Indian Ocean. *Nature*, *333*(6174), 651–655. <https://doi.org/10.1038/333651a0>
- Locke, S., & Thunell, R. C. (1988). Paleoceanographic record of the last glacial/interglacial cycle in the Red Sea and Gulf of Aden. *Palaeogeography, Palaeoclimatology, Palaeoecology*, *64*(3–4), 163–187. [https://doi.org/10.1016/0031-0182\(88\)90005-3](https://doi.org/10.1016/0031-0182(88)90005-3)
- Loeblich, A. R., & Tappan, H. (1988). Generic taxa erroneously regarded as foraminifers. In A. R. Loeblich, & H. Tappan (Eds.), *Foraminiferal genera and their classification*, (pp. 726–730). Boston, MA: Springer US. https://doi.org/10.1007/978-1-4899-5760-3_10
- Lynch-Stieglitz, J., Adkins, J. F., Curry, W. B., Dokken, T., Hall, I. R., Herguera, J. C., et al. (2007). Atlantic meridional overturning circulation during the Last Glacial Maximum. *Science*, *316*(5821), 66–69. <https://doi.org/10.1126/science.1137127>
- Lynch-Stieglitz, J., Fairbanks, R. G., & Charles, C. D. (1994). Glacial-interglacial history of Antarctic Intermediate Water: Relative strengths of Antarctic versus Indian Ocean sources. *Paleoceanography*, *9*(1), 7–29. <https://doi.org/10.1029/93PA02446>
- Lynch-Stieglitz, J., Stocker, T. F., Broecker, W. S., & Fairbanks, R. G. (1995). The influence of air-sea exchange on the isotopic composition of oceanic carbon: Observations and modeling. *Global Biogeochemical Cycles*, *9*(4), 653–665. <https://doi.org/10.1029/95GB02574>
- Mackensen, A., Hubberten, H.-W., Bickert, T., Fischer, G., & Fütterer, D. K. (1993). The $\delta^{13}\text{C}$ in benthic foraminiferal tests of *Fontbotia wuellerstorfi* (Schwager) relative to the $\delta^{13}\text{C}$ of dissolved inorganic carbon in Southern Ocean Deep Water: Implications for glacial ocean circulation models. *Paleoceanography*, *8*(5), 587–610. <https://doi.org/10.1029/93PA01291>
- Marzin, C., Kallel, N., Kageyama, M., Duplessy, J. C., & Braconnot, P. (2013). Glacial fluctuations of the Indian monsoon and their relationship with North Atlantic climate: New data and modelling experiments. *Climate of the Past*, *9*(5), 2135–2151. <https://doi.org/10.5194/cp-9-2135-2013>
- McManus, J. F., Francois, R., Gherardi, J. M., Keigwin, L. D., & Brown-Leger, S. (2004). Collapse and rapid resumption of Atlantic meridional circulation linked to deglacial climate changes. *Nature*, *428*(6985), 834–837. <https://doi.org/10.1038/nature02494>
- Mix, A. C., & Fairbanks, R. G. (1985). North Atlantic surface-ocean control of pleistocene deep-ocean circulation. *Earth and Planetary Science Letters*, *73*(2–4), 231–243. [https://doi.org/10.1016/0012-821X\(85\)90072-X](https://doi.org/10.1016/0012-821X(85)90072-X)

- Mix, A. C., Pisias, N. G., Zahn, R., Rugh, W., Lopez, C., & Nelson, K. (1991). Carbon 13 in Pacific deep and intermediate waters, 0-370 ka: Implications for ocean circulation and Pleistocene CO₂. *Paleoceanography*, 6(2), 205–226. <https://doi.org/10.1029/90PA02303>
- Monnin, E., Indermühle, A., Dällenbach, A., Flückiger, J., Stauffer, B., Stocker, T. F., et al. (2001). Atmospheric CO₂ concentrations over the last glacial termination. *Science*, 291(5501), 112–114. <https://doi.org/10.1126/science.291.5501.112>
- Murgese, D. S., & De Deckker, P. (2007). The Late Quaternary evolution of water masses in the eastern Indian Ocean between Australia and Indonesia, based on benthic foraminifera faunal and carbon isotopes analyses. *Palaeogeography, Palaeoclimatology, Palaeoecology*, 247(3–4), 382–401. <https://doi.org/10.1016/j.palaeo.2006.11.002>
- Naik, S. S., Basak, C., Goldstein, S. L., Naidu, P., & Naik, S. M. (2019). A 16-kyr record of ocean circulation and monsoon intensification from the Central Bay of Bengal. *Geochemistry, Geophysics, Geosystems*, 20. <https://doi.org/10.1029/2018GC007860>
- Naqvi, W. A., Charles, C. D., & Fairbanks, R. G. (1994). Carbon and oxygen isotopic records of benthic foraminifera from the northeast Indian Ocean: Implications for glacial-interglacial atmospheric CO₂ changes. *Earth and Planetary Science Letters*, 121(1–2), 99–110. [https://doi.org/10.1016/0012-821X\(94\)90034-5](https://doi.org/10.1016/0012-821X(94)90034-5)
- O'Malley, R. (2017). Ocean productivity. <http://www.science.oregonstate.edu/ocean.Productivity/index.php>
- Oppo, D. W., & Fairbanks, R. G. (1987). Variability in the deep and intermediate water circulation of the Atlantic Ocean during the past 25,000 years: Northern hemisphere modulation of the Southern Ocean. *Earth and Planetary Science Letters*, 86(1), 1–15. [https://doi.org/10.1016/0012-821X\(87\)90183-X](https://doi.org/10.1016/0012-821X(87)90183-X)
- Pahnke, K., Goldstein, S. L., & Hemming, S. R. (2008). Abrupt changes in Antarctic Intermediate Water circulation over the past 25,000 years. *Nature Geoscience*, 1(12), 870–874. <https://doi.org/10.1038/ngeo360>
- Pahnke, K., & Zahn, R. (2005). Southern hemisphere water mass conversion linked with North Atlantic climate variability. *Science*, 307(5716), 1741–1746. <https://doi.org/10.1126/science.1102163>
- Peltier, W. R., & Fairbanks, R. G. (2006). Global glacial ice volume and Last Glacial Maximum duration from an extended Barbados sea level record. *Quaternary Science Reviews*, 25(23–24), 3322–3337. <https://doi.org/10.1016/j.quascirev.2006.04.010>
- Peterson, C. D., Lisiecki, L. E., & Stern, J. V. (2014). Deglacial whole-ocean δ¹³C change estimated from 480 benthic foraminiferal records. *Paleoceanography*, 29, 549–563. <https://doi.org/10.1002/2013PA002552>
- Poggemann, D. W., Hathorne, E. C., Nürnberg, D., Frank, M., Bruhn, I., Reißig, S., & Bahr, A. (2017). Rapid deglacial injection of nutrients into the tropical Atlantic via Antarctic Intermediate Water. *Earth and Planetary Science Letters*, 463, 118–126. <https://doi.org/10.1016/j.epsl.2017.01.030>
- Poggemann, D. W., Nürnberg, D., Hathorne, E. C., Frank, M., Rath, W., Reißig, S., & Bahr, A. (2018). Deglacial heat uptake by the Southern Ocean and rapid northward redistribution via Antarctic Intermediate Water. *Paleoceanography and Paleoclimatology*, 33, 1292–1305. <https://doi.org/10.1029/2017PA003284>
- Rahmstorf, S. (1995). Bifurcations of the Atlantic thermohaline circulation in response to changes in the hydrological cycle. *Nature*, 378(6553), 145–149. <https://doi.org/10.1038/378145a0>
- Ramaswamy, V., Gaye, B., Shirodkar, P. V., Rao, P. S., Chivas, A. R., Wheeler, D., & Thwin, S. (2008). Distribution and sources of organic carbon, nitrogen and their isotopic signatures in sediments from the Ayeyarwady (Irrawaddy) continental shelf, northern Andaman Sea. *Marine Chemistry*, 111(3–4), 137–150. <https://doi.org/10.1016/j.marchem.2008.04.006>
- Raza, T., Ahmad, S. M., Sahoo, M., Banerjee, B., Bal, I., Dash, S., et al. (2014). Hydrographic changes in the southern Bay of Bengal during the last ~65,000 y inferred from carbon and oxygen isotopes of foraminiferal fossil shells. *Quaternary International*, 333, 77–85. <https://doi.org/10.1016/j.quaint.2014.02.010>
- Roberts, N. L., Piotrowski, A. M., McManus, J. F., & Keigwin, L. D. (2010). Synchronous deglacial overturning and water mass source changes. *Science*, 327(5961), 75–78. <https://doi.org/10.1126/science.1178068>
- Schlitzer, R. (2015). Ocean data view. <http://odv.awi.de>
- Shackleton, N. J. (1974). Attainment of isotopic equilibrium between ocean water and benthonic foraminifera genus *Uvigerina*: Isotopic changes in the ocean during the last glacial. Les méthodes quantitatives d'étude des variations du climat au cours du pléistocène, Gif-sur-Yvette. Colloque international du CNRS 219, 203–210.
- Shankar, D., Vinayachandran, P. N., & Unnikrishnan, A. S. (2002). The monsoon currents in the north Indian Ocean. *Progress in Oceanography*, 52(1), 63–120. [https://doi.org/10.1016/S0079-6611\(02\)00024-1](https://doi.org/10.1016/S0079-6611(02)00024-1)
- Shemesh, A., Hodell, D., Crosta, X., Kanfoush, S., Charles, C., & Guilderson, T. (2002). Sequence of events during the last deglaciation in Southern Ocean sediments and Antarctic ice cores. *Paleoceanography*, 17(4), 1056. <https://doi.org/10.1029/2000PA000599>
- Siddall, M., Rohling, E. J., Almogi-Labin, A., Hemleben, C., Meischner, D., Schmelzer, I., & Smeed, D. A. (2003). Sea-level fluctuations during the last glacial cycle. *Nature*, 423(6942), 853–858. <https://doi.org/10.1038/nature01690>
- Skinner, L. C., Fallon, S., Waelbroeck, C., Michel, E., & Barker, S. (2010). Ventilation of the deep Southern Ocean and deglacial CO₂ rise. *Science*, 328(5982), 1147–1151. <https://doi.org/10.1126/science.1183627>
- Skinner, L. C., Waelbroeck, C., Scrivner, A. E., & Fallon, S. J. (2014). Radiocarbon evidence for alternating northern and southern sources of ventilation of the deep Atlantic carbon pool during the last deglaciation. *Proceedings of the National Academy of Sciences*, 111(15), 5480–5484. <https://doi.org/10.1073/pnas.1400668111>
- Stocker, T. F., & Wright, D. G. (1996). Rapid changes in ocean circulation and atmospheric radiocarbon. *Paleoceanography*, 11(6), 773–795. <https://doi.org/10.1029/96PA02640>
- Stoll, H. M., Vance, D., & Arealos, A. (2007). Records of the Nd isotope composition of seawater from the Bay of Bengal: Implications for the impact of northern hemisphere cooling on ITCZ movement. *Earth and Planetary Science Letters*, 255(1–2), 213–228. <https://doi.org/10.1016/j.epsl.2006.12.016>
- Szarek, R., Kuhnt, W., Kawamura, H., & Nishi, H. (2009). Distribution of recent benthic foraminifera along continental slope of the Sunda Shelf (South China Sea). *Marine Micropaleontology*, 71(1–2), 41–59. <https://doi.org/10.1016/j.marmicro.2009.01.004>
- Talley, L. D., Pickard, G. L., Emery, W. J., & Swift, J. H. (2011). Preface. In *Descriptive physical oceanography*, (sixth ed. pp. 1–383). Boston: Academic Press.
- Thushara, V., & Vinayachandran, P. N. (2016). Formation of summer phytoplankton bloom in the northwestern Bay of Bengal in a coupled physical-ecosystem model. *Journal of Geophysical Research: Oceans*, 121, 8535–8550. <https://doi.org/10.1002/2016JC011987>
- Tisnérat-Laborde, N., Poupeau, J. J., Tannau, J. F., & Paterne, M. (2001). Development of a semi-automated system for routine preparation of carbonate samples. *Radiocarbon*, 43(2A), 299–304. <https://doi.org/10.1017/S0033822200038145>
- Toggweiler, J. R., Russell, J. L., & Carson, S. R. (2006). Midlatitude westerlies, atmospheric CO₂, and climate change during the ice ages. *Paleoceanography*, 21, GB3003. <https://doi.org/10.1029/2005PA001154>
- Tomczak, M., & Godfrey, J. S. (2003). *Regional oceanography: An introduction*. Daya Publishing House.

- Wacker, L., Fahrni, S. M., Hajdas, I., Molnar, M., Sinal, H. A., Szidat, S., & Zhang, Y. L. (2013). A versatile gas interface for routine radiocarbon analysis with a gas ion source. *Nuclear Instruments and Methods in Physics Research Section B: Beam Interactions with Materials and Atoms*, 294, 315–319. <https://doi.org/10.1016/j.nimb.2012.02.009>
- Waelbroeck, C., Levi, C., Duplessy, J. C., Labeyrie, L., Michel, E., Cortijo, E., et al. (2006). Distant origin of circulation changes in the Indian Ocean during the last deglaciation. *Earth and Planetary Science Letters*, 243(1-2), 244–251. <https://doi.org/10.1016/j.epsl.2005.12.031>
- Wais, D. P. M. (2013). Onset of deglacial warming in West Antarctica driven by local orbital forcing. *Nature*, 500, 440.
- Wen, X., Liu, Z., Wang, S., Cheng, J., & Zhu, J. (2016). Correlation and anti-correlation of the East Asian summer and winter monsoons during the last 21,000 years. *Nature Communications*, 7(1), 11999. <https://doi.org/10.1038/ncomms11999>
- Xie, R. C., Marcantonio, F., & Schmidt, M. W. (2012). Deglacial variability of Antarctic Intermediate Water penetration into the North Atlantic from authigenic neodymium isotope ratios. *Paleoceanography*, 27, PA002337. <https://doi.org/10.1029/2012PA002337>
- You, Y. (1998). Intermediate water circulation and ventilation of the Indian Ocean derived from water-mass contributions. *Journal of Marine Research*, 56(5), 1029–1067. <https://doi.org/10.1357/002224098765173455>
- You, Y., & Tomczak, M. (1993). Thermocline circulation and ventilation in the Indian Ocean derived from water mass analysis. *Deep Sea Research Part I: Oceanographic Research Papers*, 40(1), 13–56. [https://doi.org/10.1016/0967-0637\(93\)90052-5](https://doi.org/10.1016/0967-0637(93)90052-5)
- Yu, Z., Colin, C., Ma, R., Meynadier, L., Wan, S., Wu, Q., et al. (2018). Antarctic Intermediate Water penetration into the Northern Indian Ocean during the last deglaciation. *Earth and Planetary Science Letters*, 500, 67–75. <https://doi.org/10.1016/j.epsl.2018.08.006>
- Zahn, R., Winn, K., & Sarnthein, M. (1986). Benthic foraminiferal $\delta^{13}\text{C}$ and accumulation rates of organic carbon: *Uvigerina peregrina* group and *Cibicidoides wuellerstorfi*. *Paleoceanography*, 1(1), 27–42. <https://doi.org/10.1029/PA001i001p00027>